Full Length Article

Facet passivation process of high-power laser diodes by plasma cleaning and ZnO film

Yu Lan [a,b], Guowen Yang [a,b,c,*], Yuliang Zhao [a,b], Yuxian Liu [a,b], Abdullah Demir [d,*]

[a] State Key Laboratory of Transient Optics and Photonics, Xi'an Institute of Optics and Precision Mechanics, Chinese Academy of Sciences, Xi'an 710119, China
[b] University of Chinese Academy of Sciences, Beijing 100049, China
[c] Dogain Laser Technology (Suzhou) Co., Ltd., Suzhou 215123, China
[d] Bilkent University, UNAM - Institute of Materials Science and Nanotechnology, Ankara 06800, Turkey

ABSTRACT

Passivation of dangling bonds at the cleaved mirror facet and its durability are fundamental features of semiconductor lasers to obtain reliable operation with a long device lifetime. The high non-radiative recombination activity of the surface states needs to be controlled to prevent the Fermi level pinning before the deposition of mirror coating materials. Here, we report the incorporation of plasma cleaning of the facet and ZnO film as a passivation layer for the fabrication of high-power semiconductor lasers. The Argon plasma cleaning process was investigated to eliminate surface contamination without damaging the cavity surface. The ZnO passivation films were systematically studied by varying the chamber pressure and sputtering power of the radio frequency (RF) sputter coating process. We obtained homogeneous and dense ZnO films with high surface quality and optical absorption coefficient of zero. By incorporating the optimum plasma cleaning and passivation layer parameters, GaAs-based laser devices with significantly improved catastrophic optical mirror damage (COMD) power were achieved. COMD threshold was increased from 11.9 W to 20.7 W. The life test results demonstrate no failure for facet cleaned and passivated devices for more than 500 h, confirming the long-term effectiveness of the process for actual device integration.

1. Introduction

The catastrophic optical mirror damage (COMD) is a key issue limiting the reliability of laser diodes (LDs), resulting from the wafer cleaving requirement of edge-emitting LDs. When a wafer is cleaved into bars, dangling bonds are formed on the cavity surface of LDs and they are exposed air. For a clean GaAs/AlGaAs surface, such exposure to air or photons will create oxide components. These will pin the Fermi-level within the bandgap and introduce a high density of surface energy states resulting in non-radiative recombination centers. Non-radiative recombination in these states will generate a large amount of heat on the cavity surface, and the heat will accelerate the surface oxidation, thus forming a vicious cycle. This thermal effect reduces the material bandgap at the facet, enhances the absorption of light, and thus makes the cavity surface hotter. This process eventually induces the emergence of COMD for the LDs when it reaches a critical temperature [1-3]. To increase the COMD threshold of LDs, various techniques have been explored and applied to LDs such as bar cleaving in ultra-high vacuum (UHV)

environment following with in-situ passivation of the facet [4], air-cleaving with various surface passivation methods on the laser facet [5], low power density design [6], non-absorbing window technology [7], unpumped window design [8,9], quantum well intermixing [10,11], and facet cooling technique using separate pumped window [12,13]. All of these methods have raised the COMD threshold of the LDs. Although, LDs with record high output power [14,15] and performance [16,17] has been demonstrated, COMD improvement is still a major performance metric and research topic with academic and commercial interest.

Bar cleaving in UHV with in-situ facet passivation avoids native-oxide formation and hence non-radiative recombination. This approach yields a high-quality facet with long device lifetime but it has rather low productivity. This led the industry to combine laser bar cleaving in air with subsequent native oxide removal and passivation of the cleaned surfaces using standard high vacuum (HV) or UHV processing [4]. The cleaning process can be implemented by physical treatment (e.g., Ar$^+$, N$^+$ sputtering to clean the air-cleaved facets with a
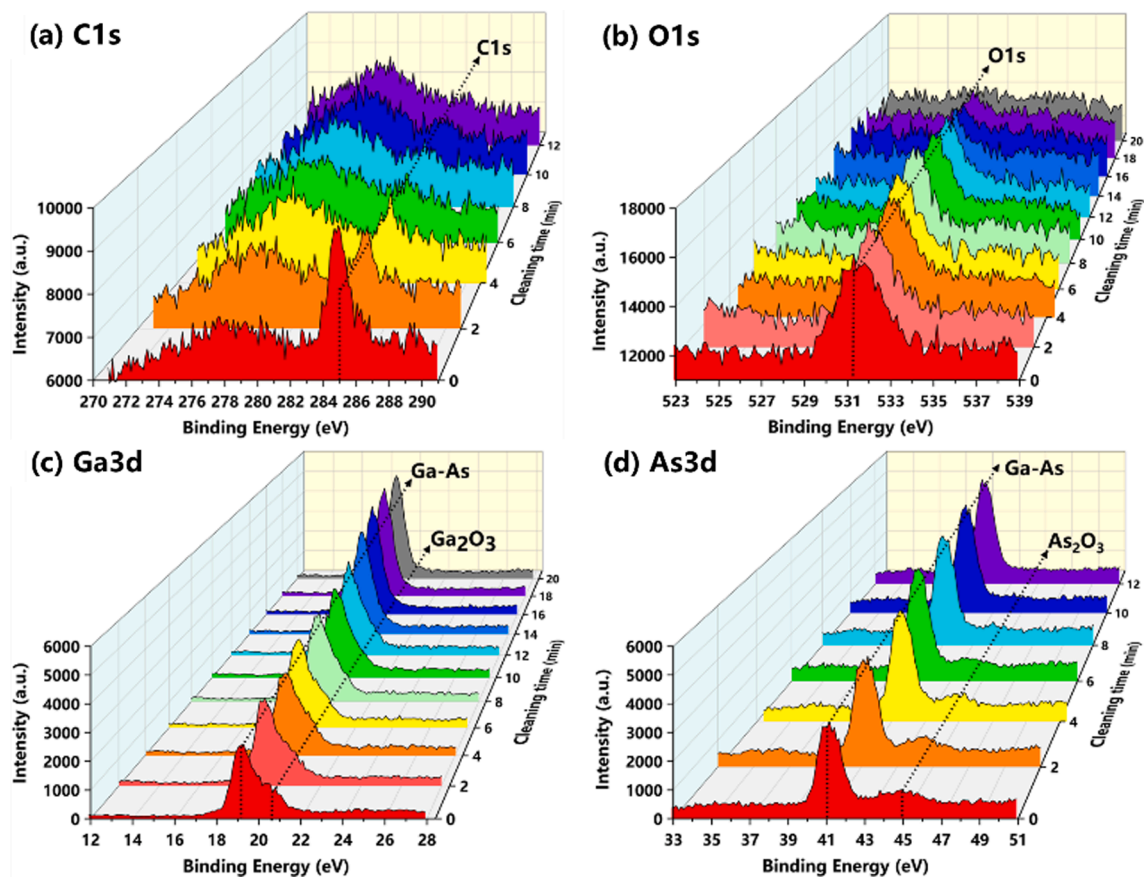

Fig. 1. The change of (a) C1s (b) O1s (c) Ga3d and (d) As3d XPS peaks during the Ar-plasma cleaning process of the LD cavity surface.

certain energy [23,24]) or chemical reaction (e.g., H^+, NH_3^+ [5,18]) methods. The physical methods inevitably introduce surface defects, which can be greatly suppressed by using suitable cleaning conditions. Among the above technologies, surface passivation methods for III-V semiconductors are possibly the most explored because of their simplicity and versatility with applications in microelectronic and optoelectronic devices [19,20]. The passivation materials should preferably have features such as wide energy bandgap, high optical transmittance, simple deposition process, high throughput and low cost. ZnSe was first chosen as the passivation material in the last century [21,22]. It was demonstrated that a ZnSe thin film deposition by molecular beam epitaxy (MBE) could prevent facet degradation for LDs, thereby improving its long-term stability and reliability under high-power operation. However, MBE growth of materials comes at the expense of high production cost and complexity with low throughput compared to the conventional physical deposition methods. ZnSe was also applied for LDs with Al-containing active region using the electron-beam evaporation method, which was demonstrated to be an effective way for improving the reliability of high-power lasers [23]. In recent years, Al_xN_y thin film sputtering combined with nitrogen plasma cleaning pretreatment was reported for GaAs-based LDs [24], and accelerated aging test results showed significantly improved device reliability. SiN_x film coated on a photonic crystal-laser diode was demonstrated by employing the sputtering method [25]. The plasma cleaning process was adopted to eliminate defects and improve the quality of the cavity surface. The COMD threshold was increased from 5 to 15.2 W resulting in higher reliability.

Of all the passivation materials, zinc oxide (ZnO) is also suitable for its great properties such as wide bandgap (3.30 eV at room temperature) [26], high laser damage threshold (1.03×10^9 W/cm^2 at 1064 nm wavelength and 2 Hz repetition rate) [27], high thermal conductivity

(100 W/m·k at room temperature) [28], high melting point (2248 K) [29], high transmittance (≥95% in the visible light wavelength range) [30], and high mechanical hardness (9.2 GPa for films annealed at 300 ℃) [31]. Although there are O atoms in Zn-O bonds, it is almost impossible for ZnO to react with Ga or As due to the large Zn-O bond strength (i.e., cohesive energy ~ 7.5 eV) [5,32], which makes ZnO a strong candidate for surface passivation. ZnO film was shown to passivate the GaAs surface with significant suppression of both Ga-O bond formation near the interface and As segregation at the interface. Trapping of carriers in oxide defects were effectively suppressed with energies near the valence band edge of GaAs [33]. Metal-organic chemical vapor deposition (MOCVD) deposited ~ 2 nm-thick ZnO passivation layer was demonstrated to effectively suppress the oxide formation and minimize the Fermi level pinning, a MOS device with leakage current reduced from 3×10^{-4} A/cm^2 to 10^{-7} A/cm^2 [34,35]. ZnO layer was shown as a strong diffusion barrier between Al_2O_3 and GaAs, effectively reducing the chance of Ga and As on the GaAs surface contacting the oxygen atoms in Al_2O_3 [36]. The application of ZnO for the passivation of AlGaAs surfaces and LDs have not been reported yet. Therefore, a systematic investigation of ZnO passivation films and their impact on LD performance are of high academic and commercial interest.

This paper focuses on the Ar plasma cleaning and ZnO passivation processes for LD facet and the impact on reliability. By implementing Ar-plasma cleaning, no obvious cleaning defects were introduced, and the oxidation and carbon contamination of LD facet can be removed to a large extent. The passivation process was optimized by adjusting chamber pressure and sputtering power to get a low absorption and low roughness ZnO film. The LD facet treatment combined with the optimized Ar-plasma cleaning and ZnO passivation conditions results in significantly enhanced COMD power and a longer accelerated lifetime,
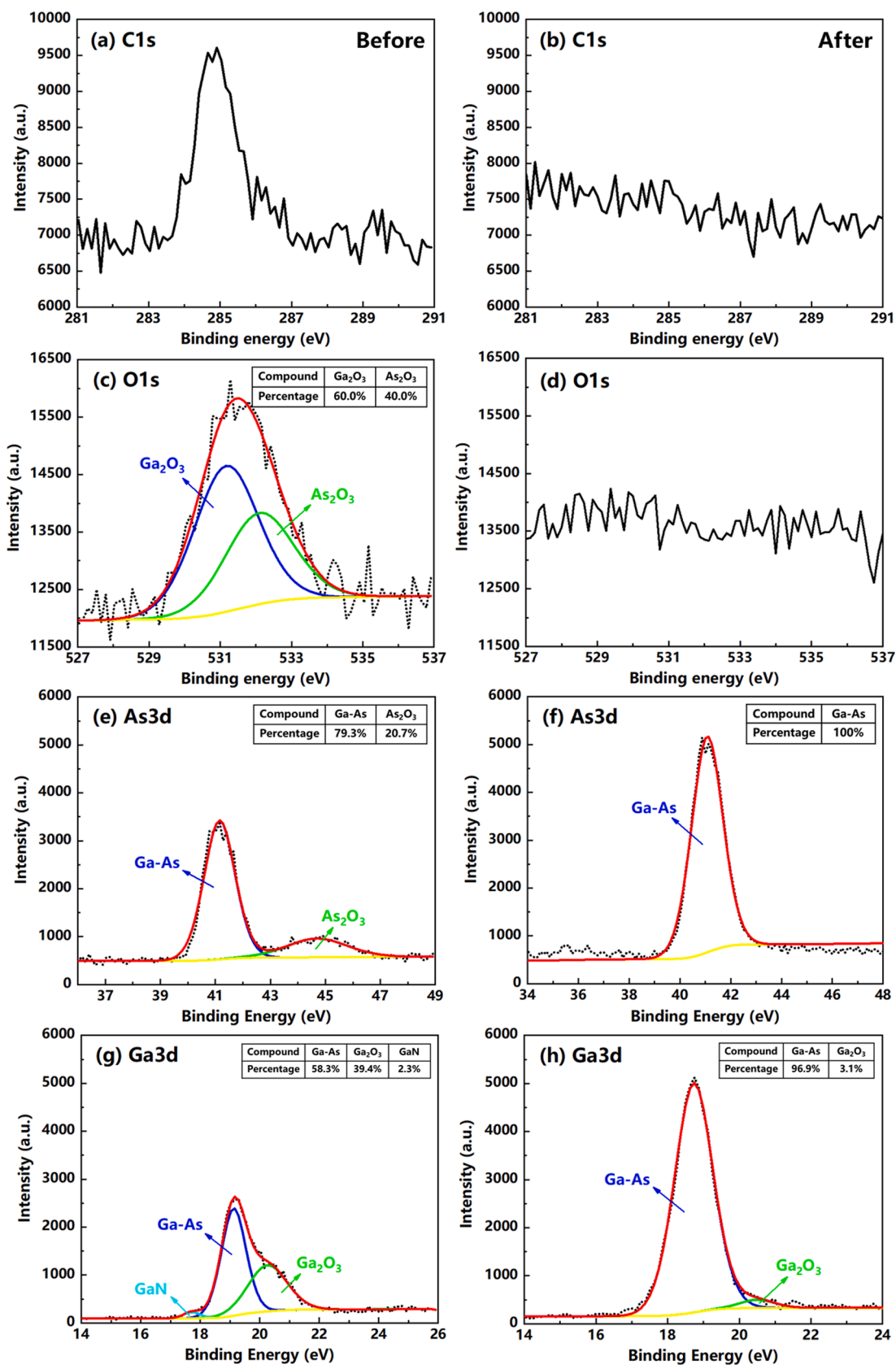
Fig. 2. The XPS spectra of C1s (a, b), O1s (c, d), Ga3d (g, h), and As3d (e, f) before (left) and after (right) the facet cleaning process.
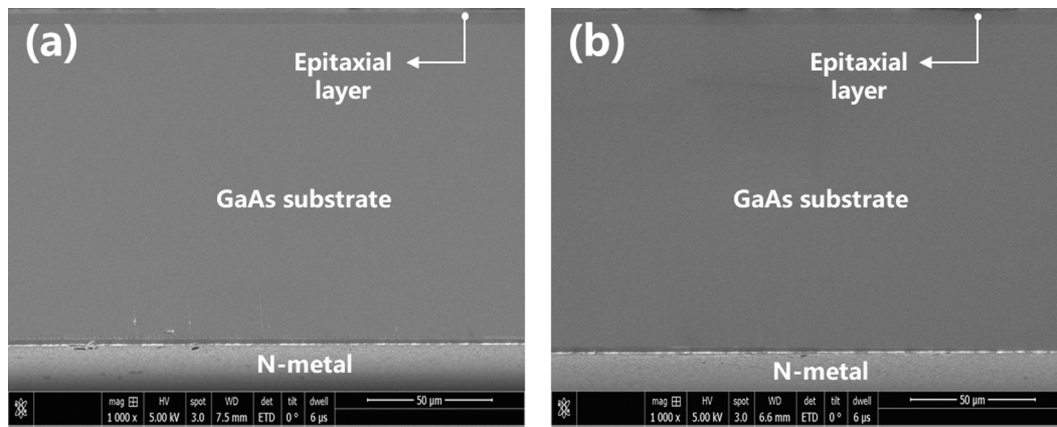
Fig. 3. The SEM images of the LD facet (a) before and (b) after Ar-plasma cleaning for 20 min.

demonstrating the effectiveness of the method for LD reliability improvement.

2. Facet cleaning process

The LDs facet is the natural cleavage surface of GaAs. The existence of dangling bonds makes the facet easy to absorb impurities such as oxygen and carbon, forming a relatively high surface state density. The native oxide forms rapidly and grows to a thickness of more than 1 nm within a few minutes [37]. This results in the Fermi level pinning effect, which will degrade the electrical and optical properties of the LDs [2,38]. To eliminate these surface states, the Ar-plasma cleaning was adopted for the LDs facet before the passivation process. This cleaning process was relatively moderate because higher plasma power and higher gas flow may introduce more defects. Based on this consideration, the cleaning conditions were set as plasma power of 30 W, the gas flow of 30 sccm, chamber pressure of 5 mTorr, and sample stage temperature control of 35 °C, which are applied on air-cleaved wafers. The surface orientation of the air-cleaved wafers used for the facet cleaning development was (1 1 0). The cleaning time needs to be controlled to maximize the removal of contaminants and oxides on the LDs facet without surface damage. We varied the cleaning duration from 0 to 20 min. The cleaned sample was transferred through a vacuum line to the XPS chamber for characterization. The XPS data were obtained using Al Kα monochromatic excitation source operated at 1486.6 eV and 25 W. In the quantitative analysis, we used CasaXPS software. Fig. 1 shows the X-ray photoelectron spectroscopy (XPS) changes of C1s, O1s, Ga3d, and As3d peaks during the cleaning process using the conditions detailed above. In the beginning, there is a strong C1s peak centered at 284.8 eV, corresponding to the C-C bond, and gradually decreased during the cleaning process. The C1s peak is close to zero after continuous cleaning for 12 min, which indicates that the carbon contamination has been fully eliminated. The O1s peak mainly contains Ga_2O_3 (centered at 530.8 eV) and As_2O_3 (centered at 531.7 eV), which are almost completely removed after cleaning for 20 min. Compared with the carbon contamination distributed only on the cleaved surfaces of the LDs, the oxide can spread into the near-surface of the bulk material, requiring a prolonged cleaning time. Fig. 1(c) and 1(d) illustrate the modification in XPS spectra of Ga3d and As3d during the cleaning process. The different cleaning time for the Ga_2O_3 (centered at 20.6 eV) and As_2O_3 (centered at 44.9 eV) is mainly due to their different proportions in the GaAs, as elaborated later in Fig. 2(c). The O1s peak is split, and the fitting demonstrates a higher Ga bond with a Ga_2O_3/As_2O_3 ratio of 1.5.

To have a more detailed analysis, Fig. 2 illustrates the impact of the procedure by comparing the XPS spectra before (left column) and after (right column) the cleaning process. As shown in Fig. 2(a) and (b), the C1s peak signal disappeared after 12 min of cleaning, indicating that the carbon contamination had been completely eliminated. Fig. 2(c) and (d) demonstrate the O1s peak change before and after 20 min of Ar-plasma cleaning. The high-resolution O1s peak can be split and fit into two different sub-peaks before cleaning. It marks that 531.2 eV and 532.1 eV correspond to Ga_2O_3 and As_2O_3, with the proportion of 60% and 40%, respectively. The binding energies and corresponding percentages of the two oxides are consistent with the previously reported results [39,40]. This indicates that the oxide layer is essentially enriched in the Ga_2O_3 phase for the naturally oxidized GaAs surface. The O1s peak almost totally disappeared after cleaning for 20 min. Fig. 2(e) is the high-resolution As3d XPS spectra of the natural cleavage surface for LD. The fitting shows two sub-peaks. The peak at 44.7 eV corresponds to As_2O_3 with a ratio of 20.7%, and the Ga-As peak is centered at 41.2 eV with a ratio of 79.3%. The As_2O_3 peak disappeared after cleaning for 12 min, as shown in Fig. 2(f). Fig. 2(g) is the XPS spectra of Ga3d for the as-cleaved surface. Three distinctive subpeaks are identified as Ga-As (19.2 eV), Ga_2O_3 (20.5 eV), GaN (17.7 eV) with the corresponding proportions of 58.3%, 39.4%, and 2.3%, respectively. The appearance of the GaN peak is likely due to the nitriding effect of air on the cavity surface. After cleaning for 20 min (Fig. 2h), the GaN peak was removed, and the Ga_2O_3 peak was dramatically reduced to 3.1%. The removal of Ga_2O_3 slowed down with process times longer than 14 min. Ga_2O_3 was not entirely eliminated even for longer than 20 min of processing. Since the extended duration of physical cleaning times may inevitably introduce non-radiative surface defects, our study's cleaning time was limited to 20 min. Fig. 3 shows the SEM picture of the LD facet before and after argon
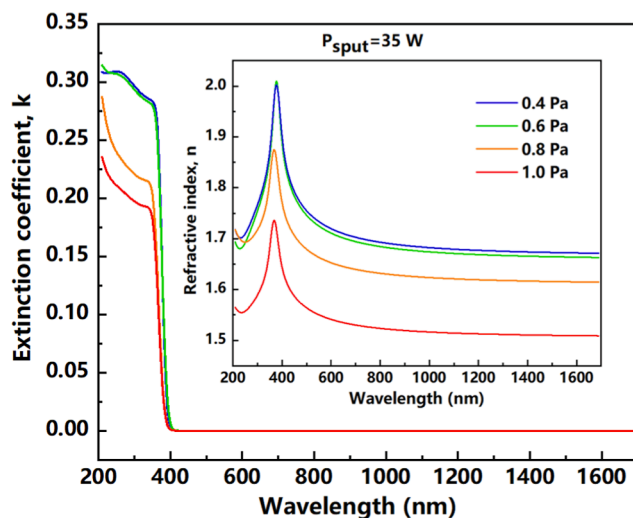

Fig. 4. The influence of chamber pressure on extinction coefficient and refractive index (the inset) of the ZnO films at the sputtering power of 35 W.
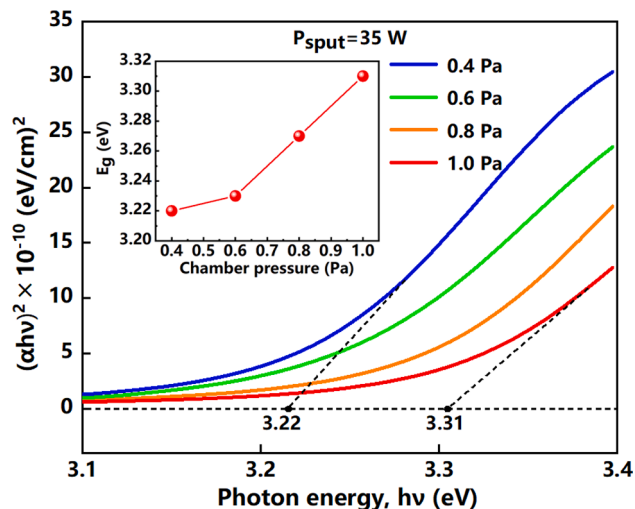
Fig. 5. The relationship of $(\alpha h\nu)^2$ and photon energy (hν) for the ZnO films with the various chamber pressure at 35 W. The inset shows the optical bandgap as a function of the chamber pressure.

plasma cleaning for 20 min. The cleaning process induced no apparent defect at the facet surface.

3. ZnO passivation study

Undoped (1 0 0) GaAs substrates were first immersed in H_2O_2-NH_4OH-H_2O liquid for 30 s with the ratio of 1:1:2 to degrease the wafers and remove surface oxide. Then, they were rinsed in deionized water for 1 min and dried by nitrogen. A radio-frequency (RF) plasma-enhanced magnetron sputtering machine was employed to obtain thin ZnO films. The deposition was carried out at room temperature, where the chamber pressure was varied in the range of 0.4 to 1.0 Pa. The sputtering power was varied between 20 and 60 W to obtain the optimum ZnO deposition conditions. 20 nm thick ZnO films were deposited for the characterization. GaAs wafers were used to characterize the refractive index (n) and extinction coefficient (k) of the films. For optical band gap (E_g) measurements, ZnO was deposited on high transmittance high purity Al_2O_3 substrates. Refractive index and extinction coefficient data

were obtained using a spectroscopic ellipsometer (SE).

3.1. Chamber pressure

Fig. 4 shows the influence of chamber pressure on the refractive index and extinction coefficient. The sputtering power (P_{sput}) was kept at 35 W to better compare the effect of different chamber pressures. With higher pressure, the refractive index reduces in the wavelength range of 200 nm to 1700 nm. The higher amount of argon at higher pressure increases the collision between the argon and the sputtered ZnO particles. This results in a smaller mean free path and reduced kinetic energy of the ZnO particles reaching the substrate. The adhesion of the ZnO film to the substrate and the structural compactness will decrease, and all these factors together lead to reduced density and lower refractive index of the film. The changing trend of the extinction coefficient with pressure is the same as the refractive index. The corresponding extinction coefficient under different pressure conditions is zero when the wavelength is longer than 400 nm. The k = 0 corresponds to ultra-low optical absorption and is critical for improved COMD levels [25].

According to the interband absorption theory, the optical band gap (E_g) of ZnO films was calculated based on the following relation [41]:

$$(\alpha h\nu) = A(h\nu - E_g)^n \tag{1}$$

where α is absorption coefficient of the film, hν is the incident photon energy, A is a constant, n is determined by the transition type, being 1/2 for the direct transition, 3/2 for the direct forbidden transition, 2 for the indirect transition, and 3 for the indirect forbidden transition [42].

The plotting of $(\alpha h\nu)^{1/n}$ against hν and then E_g is obtained by extrapolating the curve to the hν intercept. Fig. 5 shows the results of $(\alpha h\nu)^2$ versus photon energy for the ZnO films under different chamber pressures. The results obey the equation (1) with n = 1/2, indicating a direct transition as expected for the band-edge region [43]. As the chamber pressure increased from 0.4 Pa to 1.0 Pa, the optical band gap E_g also increased from 3.22 eV to 3.31 eV. Burstein-Moss effect is commonly considered for such an increase in the bandgap of the film due to the carrier concentration effects [44]. However, this is not related to our case since no such doping is involved in our process. We speculate that this change might be related to the stoichiometry of the deposited materials.

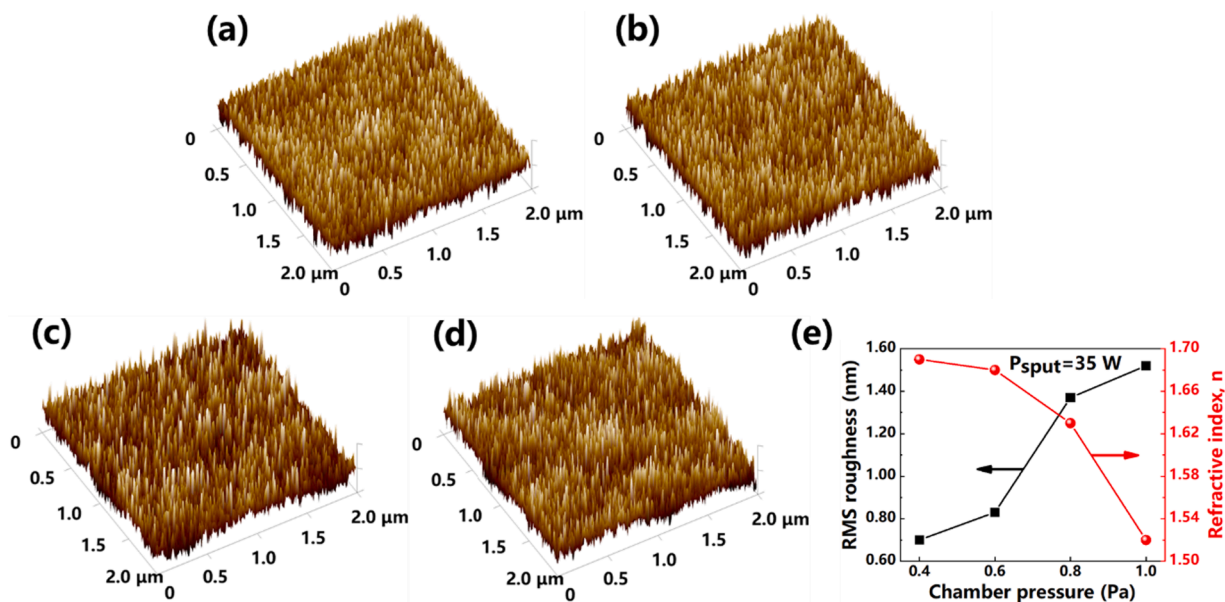Surface images obtained by three-dimensional atomic force

Fig. 6. The three-dimensional AFM morphology of the ZnO films (2 μm × 2 μm), sputtered by different chamber pressures. (a) 0.4 Pa, (b) 0.6 Pa, (c) 0.8 Pa, (d) 1.0 Pa. (e) RMS roughness and refractive index change with pressure at $P_{sput.}$ = 35 W.
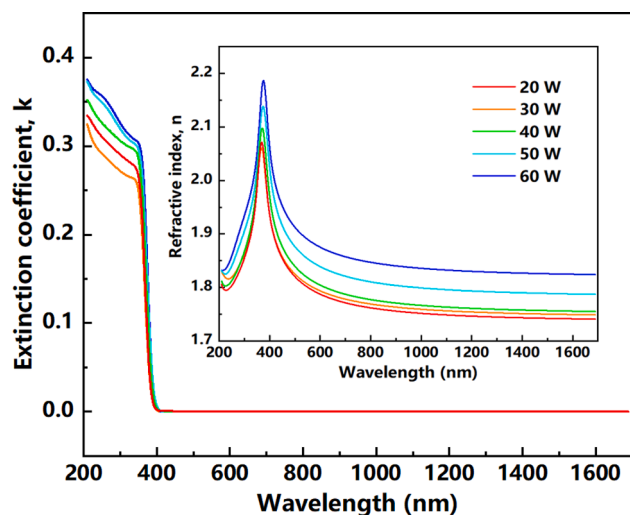
Fig. 7. The influence of sputtering power on extinction coefficient and refractive index (the inset) of the ZnO films at the chamber of 0.4 Pa.

a downward trend as the wavelength increases from 400 nm to 1700 nm. Besides, the refractive index of the ZnO film increases with the rise of the sputtering power. This can be explained by the fact that when the argon plasma obtains higher energy, on the one hand, the number of ZnO particles sputtered per unit time will increase, and more particles can directly collide to form crystal nuclei. On the other hand, the sputtered ZnO particles have higher energy, which leads to higher migration kinetic energy of these particles on the surface of the substrate. Therefore, surface diffusion and bonding can occur more easily to form crystal nuclei, and these crystal nuclei are the key to creating a denser structure and higher refractive index ZnO film. Fig. 8 presents the AFM characterization results. The measured RMS roughness values show a decreasing trend as the sputtering power increases, consistent with the refractive index results. It is mainly due to the denser film structure with higher sputtering power.
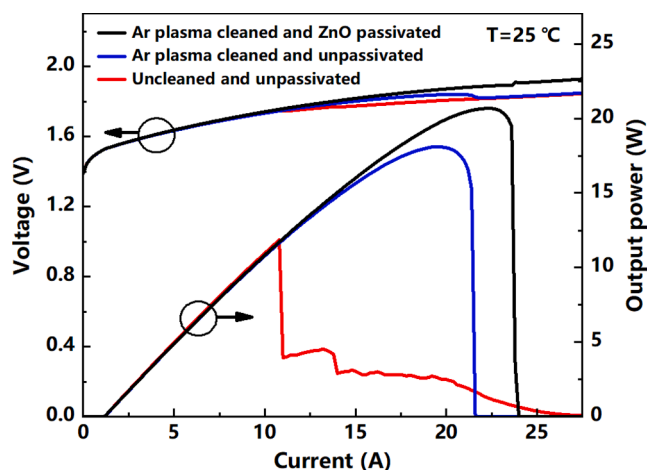
microscopy (AFM) show different morphology for the ZnO/GaAs films, as shown in Fig. 6. The root-mean-square (RMS) roughness (R_{rms}) of the ZnO/GaAs films under different chamber pressures are 0.70 nm (0.4 Pa), 0.83 nm (0.6 Pa), 1.37 nm (0.8 Pa), and 1.52 nm (1.0 Pa). The increased R_{rms} with pressure indicates degradation in the surface quality of the film. The ZnO particles deposited on the GaAs surface do not gain enough energy when the chamber pressure is too high. Thus, these particles cannot spread, combine and form large crystal grains, which is the necessary process of the ZnO film growth. Fig. 6(e) shows the variation of RMS roughness and refractive index with pressure. A low surface roughness corresponds to a high optical refractive index and indicates a better film quality at 0.4 Pa.

3.2. Sputtering power

Fig. 7 depicts the refractive index and extinction coefficient versus wavelength for the ZnO films under different sputtering power and maintaining the chamber pressure of 0.4 Pa. The refractive index shows

Fig. 9. Curves of power versus current for three different facet treatment methods.
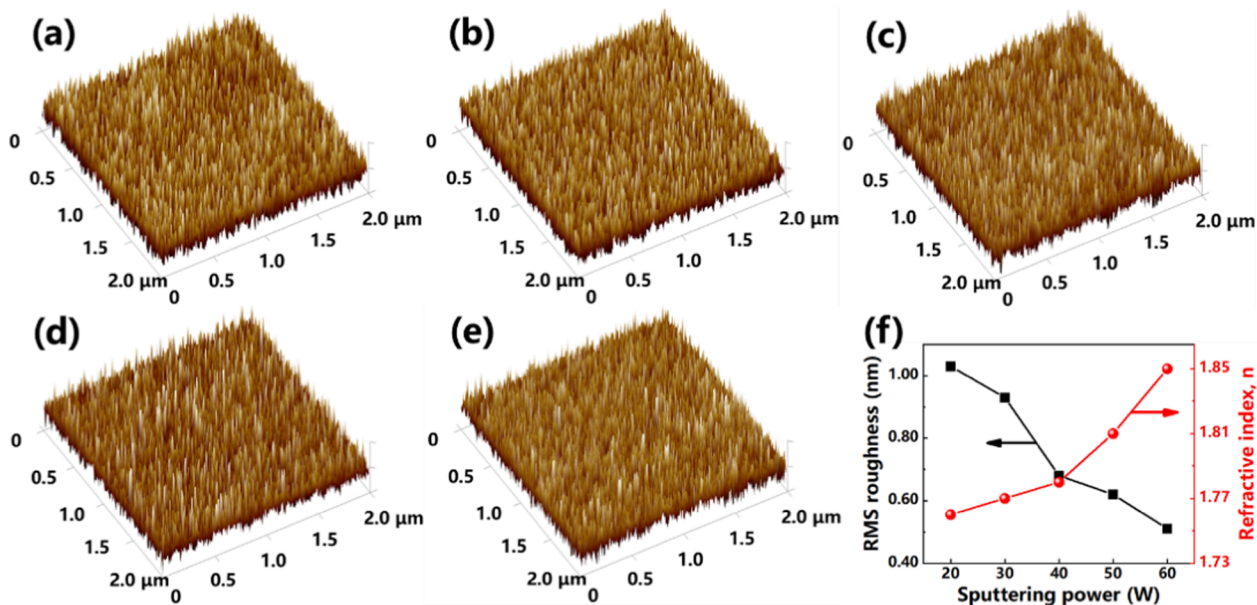

Fig. 8. The AFM morphology of the ZnO films at 0.4 Pa under sputtering power levels of (a) 20 W, (b) 30 W, (c) 40 W, (d) 50 W, (e) 60 W. (f) The variation of RMS roughness and refractive index with sputtering power.
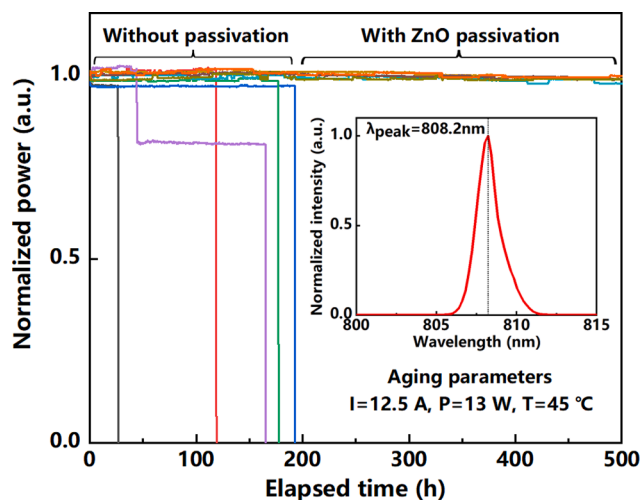
Fig. 10. Accelerated aging test for LDs with and without ZnO passivation after Ar-cleaning. The inset shows a typical spectrum of a laser diode.

4. Results of LDs reliability with Ar-cleaning and ZnO passivation film

We fabricated high-power GaAs-based LDs with AlGaAs waveguide and InAlGaAs single QW active region. The LDs have a cavity length of 4 mm and a waveguide width of 200 μm for laser emission around 808 nm. We applied three sets of conditions on these LDs to prove the effectiveness of the cleaning and passivation process presented herein. Our goal was to test their COMD levels and implement an aging test to understand the effectiveness of the applied processes. In the beginning, LDs in all the sets were cleaved in an atmospheric environment. In the end, the anti-reflective (AR) and high-reflective (HR) mirror coating were deposited with high transmittance (SiO$_2$) and high reflectivity films (SiO$_2$/Si$_3$N$_4$/Si multilayer). In the first set, the mirror coating process was applied without any cleaning and passivation process. As shown in Fig. 9 at 25 °C heat-sink temperature, these LDs demonstrated the lowest COMD power with a typical value of 11.9 W. In the second set, the LDs facets were cleaned by Ar-plasma before the mirror coating step. This treatment increased the COMD level to 18.1 W. In the third set, the LDs were applied with the optimized Ar-cleaning and ZnO passivation film (12 nm thick) before coating. A vacuum piping connects the cleaning and the sputtering equipment to eliminate the contamination and oxidation of the cleaned facet in the transfer process. The cleaning combined with ZnO passivation procedures increased the COMD level to 20.7 W, which happened after the power rollover. The COMD occurred after power rollover both for the ZnO passivated, and unpassivated LDs with facet cleaning indicating the effectiveness of the above cleaning process. The difference in their thermal rollover can be attributed mainly to chip-to-chip variation. Life test results are essential to clarify the critical benefit and robustness of the passivation process. Hence, the LDs were tested to investigate the long-term strength and reliability of the applied process. Fig. 10 shows the normalized power of five unpassivated and five passivated LDs aged without burn-in in a constant current regime at 12.5 A (13 W) and 45 °C over a time of 500 h. The inset presents a typical spectrum of the LDs with a peak wavelength of 808 nm. The uncleaned and unpassivated devices do not even reach this condition, as can be expected from Fig. 9. The LDs treated by only Ar-cleaning work but fail within 200 h. In contrast, five passivated LDs achieve an accelerated lifetime of more than 500 h. The results in Figs. 9 and 10 confirm the effectiveness of the implemented process. In our life test, the output power of 13 W is above the industry standard operating power level of around 10 W for such an LD (i.e., waveguide width of ∼ 200 μm). We believe that the reliable output power level can be improved through further optimization of the cleaning and passivation
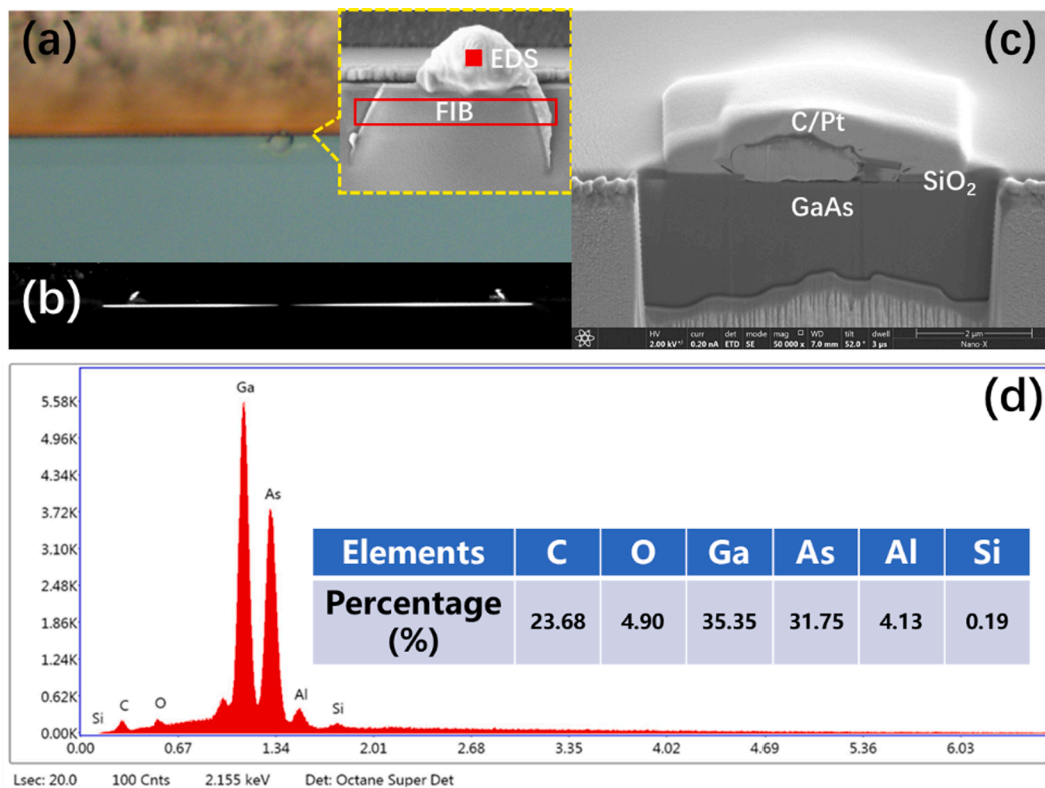

Fig. 11. (a) Optical micrography of the front facet for the failed device caused by COMD. The inset is the SEM image of the defect position. (b) Electroluminescence (EL) image of the front facet. (c) FIB microscopy for the defect region as shown in the red box in (a). (d) EDS analysis of the spilled substance showed in (a). (For interpretation of the references to colour in this figure legend, the reader is referred to the web version of this article.)

process using the results of this work as a guideline.

5. Failure analysis for COMD device

After the accelerated aging for different groups, we have chosen one failed device (Ar-cleaned, unpassivated) for analysis. First, the morphology of the cavity surface was observed by using optical microscopy. A COMD point is apparent in the epitaxial layer in Fig. 11(a). Fig. 11(b) is the electroluminescence (EL) image for the AR surface of the failed device. The non-luminous position corresponds to a defect point in Fig. 11(a). A scanning electron microscope (SEM) was used to characterize the morphology of the COMD point. To examine the interface and epitaxial layers affected by COMD, we employed focused ion beam (FIB) microscopy by a cut through the center of the facet defect, which can be seen in Fig. 11(c). There are some holes and fused AlGaAs under the front facet coating, where the AR film is also locally deformed and burned. The AR film was torn apart by the spilled material inside, which is mainly composed of AlGaAs based on the energy-dispersive X-ray spectroscopy (EDS) as shown in Fig. 11(d). This indicates that COMD occurs when the facet temperature reaches the melting point of the semiconductor material. Two factors can cause facet heating, including optical absorption of the laser near the facet and non-radiative recombination of electrons and holes at the surface states of the cleaved facet [45]. The spilled substance was due to the bulk material being melted and re-solidified, causing many layers to mix and change their properties to an amorphous state [46].

6. Conclusion

We presented a novel process for facet passivation of air-cleaved high-power LDs. Ar-plasma was applied for laser facet cleaning, and ZnO film was used as a passivation layer. The facet surface cleaning process was optimized by controlling the cleaning time and utilizing modest plasma energy. No formation of obvious defects after cleaning indicates high cleaning quality. We obtained the optimized coating condition for the passivation layer by controlling the chamber pressure and sputtering power. The optimized ZnO film had a low surface roughness with zero optical absorption (wavelength at 400 to 1700 nm). The LDs combined with the optimized cleaning and ZnO passivation conditions were implemented for high-power 808 nm LDs. We achieved an average COMD level of 20.7 W and an accelerated lifetime of more than 500 h.

CRediT authorship contribution statement

Yu Lan: Investigation, Data curation, Writing – original draft, Writing – review & editing. **Guowen Yang:** Supervision, Project administration, Funding acquisition. **Yuliang Zhao:** Investigation. **Yuxian Liu:** Investigation. **Abdullah Demir:** Supervision, Writing – original draft, Writing – review & editing.

Declaration of Competing Interest

The authors declare that they have no known competing financial interests or personal relationships that could have appeared to influence the work reported in this paper.

Acknowledgements

References

[1] Sanayeh, M. Bou, et al., The physics of catastrophic optical damage in high-power AlGaInP laser diodes, Semiconductor Lasers and Laser Dynamics III, Vol. 6997, International Society for Optics and Photonics, 2008.
[2] M. Bou Sanayeh, P. Brick, W. Schmid, B. Mayer, M. Müller, M. Reufer, K. Streubel, S. Schwirzke-Schaaf, J.W. Tomm, A. Danilewsky, G. Bacher, Defect investigation and temperature analysis of high-power AlGaInP laser diodes during catastrophic optical damage, J. Mater. Sci.: Mater. Electron. 19 (S1) (2008) 155–159.
[3] J.W. Tomm, M. Ziegler, M. Hempel, T. Elsaesser, Mechanisms and fast kinetics of the catastrophic optical damage (COD) in GaAs-based diode lasers, Laser Photonics Rev. 5 (3) (2011) 422–441.
[4] P.W. Epperlein, Semiconductor laser engineering, reliability and diagnostics: a practical approach to high power and single mode devices, John Wiley & Sons, 2013.
[5] L.u. Zhou, B. Bo, X. Yan, C. Wang, Y. Chi, X. Yang, Brief review of surface passivation on III-V semiconductor, Crystals 8 (5) (2018) 226.
[6] I.B. Petrescu-Prahova, et al., High d/gamma values in diode laser structures for very high power, High-Power Diode Laser Technology and Applications VII, Vol. 7198. International Society for Optics and Photonics, 2009.
[7] R.M. Lammert, et al., High power (> 10W from 100μm aperture) high reliability 808nm InAlGaAs broad area laser diodes, Electron. Lett. 42 (9) (2006) 535–536.
[8] G. Yang, G.M. Smith, M.K. Davis, D.A.S. Loeber, M. Hu, C. Zah, R. Bhat, Highly reliable high-power 980-nm pump laser, IEEE Photonics Technol. Lett. 16 (11) (2004) 2403–2405.
[9] J. Hendrix, G. Morthier, R. Baets, Influence of laser parameters and unpumped regions near the facets on the power level for catastrophic optical damage in short wavelength lasers, IEE Proc.-Optoelectron. 144 (2) (1997) 109–114.
[10] K. Zheng, et al., High power red-light GaInP/AlGaInP laser diodes with nonabsorbing windows based on Zn diffusion-induced quantum well intermixing, Chin. Opt. Lett. 4 (1) (2006) 27–29.
[11] S. Arslan, A. Demir, S. Sahin, A. Aydınlı, Conservation of quantum efficiency in quantum well intermixing by stress engineering with dielectric bilayers, Semicond. Sci. Technol. 33, 025001 (2018).
[12] Arslan, Seval, et al. Facet Cooling in High-Power InGaAs/AlGaAs Lasers, IEEE Photonics Technol. Lett. 31.1 (2018): 94-97.
[13] Demir, Abdullah, et al., Reduced facet temperature in semiconductor lasers using electrically pumped windows, High-Power Diode Laser Technology XVII, Vol. 10900. International Society for Optics and Photonics, 2019.
[14] A. Demir, M. Peters, R. Duesterberg, V. Rossin, E. Zucker, Semiconductor laser power enhancement by control of gain and power profiles, IEEE Photonics Technol. Lett. 27 (20) (2015) 2178–2181.
[15] Demir, Abdullah, et al., 29.5 W continuous wave output from 100um wide laser diode, High-Power Diode Laser Technology and Applications XIII, Vol. 9348, International Society for Optics and Photonics, 2015.
[16] Y.u. Lan, G. Yang, Y. Liu, Y. Zhao, Z. Wang, T.e. Li, A. Demir, 808 nm broad-area laser diodes designed for high efficiency at high-temperature operation, Semicond. Sci. Technol. 36 (10) (2021) 105012.
[17] Y. Liu, et al., High-power operation and lateral divergence angle reduction of broad-area laser diodes at 976 nm, Opt. Laser Technol. 141 (2021), 107145.
[18] J.E. Boschker, et al., Stability of ZnSe-passivated laser facets cleaved in air and in ultra-high vacuum. 2021 27th International Semiconductor Laser Conference (ISLC). IEEE, 2021.
[19] H. Hasegawa, M. Akazawa, Surface passivation technology for III–V semiconductor nanoelectronics, Appl. Surf. Sci. 255 (3) (2008) 628–632.
[20] O.P. Agnihotri, S.C. Jain, J. Poortmans, J. Szlufcik, G. Beaucarne, J. Nijs, R. Mertens, Advances in low temperature processing of silicon nitride based dielectrics and their applications in surface passivation and integrated optical devices, Semicond. Sci. Technol. 15 (7) (2000) R29–R40.
[21] N. Chand, W.S. Hobson, J.F. de Jong, P. Parayanthal, U.K. Chakrabarti, ZnSe for mirror passivation of high power GaAs based lasers, Electron. Lett. 32 (17) (1996) 1595.
[22] A.V. Syrbu, V.P. Yakovlev, G.I. Suruceanu, A.Z. Mereutza, L.J. Mawst, A. Bhattacharya, M. Nesnidal, J. Lopez, D. Botez, ZnSe-facet-passivated InGaAs/InGaAsP/InGaP diode lasers of high CW power and 'wallplug'efficiency, Electron. Lett. 32 (4) (1996) 352.
[23] X. Shu, C. Xu, Z. Tian, G. Shen, ZnSe by electron-beam evaporation used for facet passivation of high power laser diodes, Solid-State Electron. 49 (12) (2005) 2016–2017.
[24] Lu Zhou, Xin Gao, Yunhua Wang, Liuyang Xu, Baoshan Jia, Duanyuan Bai, Baoxue Bo, Facet passivation of GaAs based LDs by N_2 plasma pretreatment and RF sputtered Al_xN_y film coating, J. Lightwave Technol. 31 (13) (2013) 2279–2283.
[25] Y. Wang, H. Qu, Y. Wang, F. Dong, Z. Chen, W. Zheng, Radio Frequency Plasma-Enhanced Reactive Magnetron Sputtering Deposition of α-SiNx on Photonic Crystal—Laser Diodes for Facet Passivation, ACS Omega 4 (23) (2019) 20205–20211.
[26] M. Caglar, S. Ilican, Y. Caglar, F. Yakuphanoglu, Electrical conductivity and optical properties of ZnO nanostructured thin film, Appl. Surf. Sci. 255 (8) (2009) 4491–4496.
[27] N. Lameche, S. Bouzid, M. Hamici, M. Boudissa, S. Messaci, K. Yahiaoui, Effect of indium doping on the optical properties and laser damage resistance of ZnO thin films, Optik 127 (20) (2016) 9663–9672.
[28] Ü. Özgür, Y.I. Alivov, C. Liu, A. Teke, M.A. Reshchikov, S. Doğan, V. Avrutin, S.-J. Cho, H. Morkoç, A comprehensive review of ZnO materials and devices, J. Appl. Phys. 98 (4) (2005) 041301.

[29] F.K. Shan, B.C. Shin, S.W. Jang, Y.S. Yu, Substrate effects of ZnO thin films prepared by PLD technique, J. Eur. Ceram. Soc. 24 (6) (2004) 1015–1018.

[30] Q.H. Li, D. Zhu, W. Liu, Y.i. Liu, X.C. Ma, Optical properties of Al-doped ZnO thin films by ellipsometry, Appl. Surf. Sci. 254 (10) (2008) 2922–2926.

[31] C.-Y. Yen, S.-R. Jian, G.-J. Chen, C.-M. Lin, H.-Y. Lee, W.-C. Ke, Y.-Y. Liao, P.-F. Yang, C.-T. Wang, Y.-S. Lai, J.-C. Jang, J.-Y. Juang, Influence of annealing temperature on the structural, optical and mechanical properties of ALD-derived ZnO thin films, Appl. Surf. Sci. 257 (17) (2011) 7900–7905.

[32] H. Morkoç, Ü. Özgür, Zinc oxide: fundamentals, materials and device technology, John Wiley & Sons, 2008.

[33] Y.-C. Byun, S. Choi, Y. An, P.C. McIntyre, H. Kim, Tailoring the interface quality between HfO$_2$ and GaAs via in situ ZnO passivation using atomic layer deposition, ACS Appl. Mater. Interfaces 6 (13) (2014) 10482–10488.

[34] S. Kundu, T. Shripathi, P. Banerji, Interface engineering with an MOCVD grown ZnO interface passivation layer for ZrO$_2$–GaAs metal–oxide–semiconductor devices, Solid State Commun. 151 (24) (2011) 1881–1884.

[35] S. Kundu, Y. Anitha, S. Chakraborty, P. Banerji, Interface studies on high-k/GaAs MOS capacitors by deep level transient spectroscopy, J. Vacuum Sci. Technol. B, Nanotechnol. Microelectron.: Mater., Process., Meas. Phenomena 30 (5) (2012) 051206.

[36] C. Liu, Y.-M. Zhang, Y.-M. Zhang, H.-L. Lü, Interfacial characteristics of Al/Al$_2$O$_3$/ZnO/n-GaAs MOS capacitor, Chin. Phys. B 22 (7) (2013) 076701.

[37] S. Matteson, R.A. Bowling, Experimental investigation of GaAs surface oxidation, MRS Online Proceedings Library (OPL) 48 (1985).

[38] T. Yuasa, M. Ogawa, K. Endo, H. Yonezu, Degradation of (AlGa)As DH lasers due to facet oxidation, Appl. Phys. Lett. 32 (2) (1978) 119–121.

[39] Ishikawa, Toshifumi, Hideaki Ikoma, X-ray photoelectron spectroscopic analysis of the oxide of GaAs, Japanese J. Appl. Phys. 31.12R (1992): 3981.

[40] V.M. Mikoushkin, V.V. Bryzgalov, S.Y. Nikonov, A.P. Solonitsyna, D.E. Marchenko, Composition and band structure of the native oxide nanolayer on the ion beam treated surface of the GaAs wafer, Semiconductors 52 (5) (2018) 593–596.

[41] S.T. Tan, B.J. Chen, X.W. Sun, W.J. Fan, H.S. Kwok, X.H. Zhang, S.J. Chua, Blueshift of optical band gap in ZnO thin films grown by metal-organic chemical-vapor deposition, J. Appl. Phys. 98 (1) (2005) 013505.

[42] A.N. Banerjee, C.K. Ghosh, K.K. Chattopadhyay, H. Minoura, A.K. Sarkar, A. Akiba, A. Kamiya, T. Endo, Low-temperature deposition of ZnO thin films on PET and glass substrates by DC-sputtering technique, Thin Solid Films 496 (1) (2006) 112–116.

[43] J. Lu, Z. Ye, L. Wang, J. Huang, B. Zhao, Structural, electrical and optical properties of N-doped ZnO films synthesized by SS-CVD, Mater. Sci. Semicond. Process. 5 (6) (2002) 491–496.

[44] E. Burstein, Anomalous optical absorption limit in InSb, Phys. Rev. 93 (3) (1954) 632–633.

[45] J.-I. Hashimoto, et al., A highly reliable GaInAs-GaInP 0.98-μm window laser, IEEE J. Quantum Electron. 36 (8) (2000) 971–977.

[46] M. Bou Sanayeh, A. Jaeger, W. Schmid, S. Tautz, P. Brick, K. Streubel, G. Bacher, Investigation of dark line defects induced by catastrophic optical damage in broad-area AlGaInP laser diodes, Appl. Phys. Lett. 89 (10) (2006) 101111.